Title
STRAIN HARDENING OF SINGLE ALUMINUM CRYSTALS DURING POLYSLIP

Authors
Mukherjee, A.K.
Mote, J.D.
Dorn, J.E.

Publication Date
1965-01-15

UCRL-11888

University of California

Ernest O. Lawrence Radiation Laboratory

STRAIN HARDENING OF SINGLE ALUMINUM CRYSTALS DURING POLYSLIP

Berkeley, California

DISCLAIMER

Trans. AIME UCRL-11888

UNIVERSITY OF CALIFORNIA
Lawrence Radiation Laboratory
Berkeley, California

AEC Contract No. W-7405-eng-48

STRAIN HARDENING OF SINGLE ALUMINUM CRYSTALS DURING POLYSLIP

A. K. Mukherjee,[1] J. D. Mote[2] and J. E. Dorn[3]

January 15, 1965

[1]Postdoctoral Research Fellow of the Inorganic Materials Research Division of the Lawrence Radiation Laboratory, University of California, Berkeley.

[2]Formerly Research Metallurgist of the Inorganic Materials Research Division of the Lawrence Radiation Laboratory, University of California, Berkeley; now Research Metallurgist, Sandia Corporation, Albuquerque.

[3]Professor of Materials Science of the Department of Mineral Technology, College of Engineering and Research Metallurgist of the Inorganic Materials Research Division of the Lawrence Radiation Laboratory, University of California, Berkeley.

STRAIN HARDENING OF SINGLE ALUMINUM CRYSTALS DURING POLYSLIP

A. K. Mukherjee, J. D. Mote and J. E. Dorn

Inorganic Materials Research Division, Lawrence Radiation Laboratory, and Department of Mineral Technology, College of Engineering, University of California, Berkeley, California

January 15, 1965

ABSTRACT

Investigations were carried out on the effect of polyslip on the strain hardening of Al single crystals. The orientations investigated were those for which the tensile axis was in the [001], [$\bar{1}$11], [$\bar{1}$12] and [012] directions plus another for which the Schmid angles for $\{\bar{1}11\}$ <110> slip were $90-\chi_o=\lambda_o = 45° \pm 1°$. The experimental data were analysed on a model based on the intersection of dislocations with particular emphasis on the effect of polyslip on the activation volume for intersection. It is shown that the rate of strain hardening increases for those orientations wherein attractive dislocation intersections occur and that those orientations which produce the greater number of such intersections exhibit the greater strain hardening. Good correlation of the data is obtained with the concept that attractive junctions, as proposed by Saada, play an important role in accounting for the rate of strain hardening.

I. INTRODUCTION

Existing concepts on the nature and cause of strain hardening in face-centered cubic metals have been deduced principally from experiments on the deformation of single crystals under single slip. The effect of crystal orientation on the shapes of the stress-strain curves for single slip have been summarized by Seeger[1] and more recently by Clarebrough and Hargreaves.[2] Tensile specimens whose axes fall near the center of the [001]-[011] line of the standard triangle of the stereographic projection exhibit the longest range of easy glide (Stage I) and the lowest rates of linear hardening (Stage II) whereas specimens whose axes lie near the [001]-[$\bar{1}$11] line of the standard triangle have limited or no easy glide range and exhibit somewhat higher linear strain-hardening rates. Specimens whose axes lie near the [001] or the [$\bar{1}$11] poles do not exhibit easy glide and have the highest rates of linear hardening. Kocks[3] has shown that the highest rates of linear hardening occur under polyslip when the tensile axis coincides with the [$\bar{1}$11] or the [001] pole.

Since the rate of strain hardening is sensitive to specimen orientation and the incidence of polyslip, these relationships might help to discriminate between various dislocation models for strain hardening in face-centered cubic metals. Previous attempts to analyze the effect of orientation on strain hardening,[1, 2, 3] however, did not provide a unique answer to this problem. Consequently the present investigation was undertaken wherein additional data, particularly that for the effect of polyslip on the activation volume for intersection, was also determined in order to provide more complete information on the details of strain hardening. Whereas

analyses of these data reveal that several recommended models for strain hardening are at variance with the facts, good correlation of the data is obtained with the concept that attractive junctions[4] play an important role in accounting for the rate of strain hardening.

II. EXPERIMENTAL APPROACH

Seeger[1] demonstrated that slip in face-centered cubic crystals at low temperatures is dependent on thermally activated intersection of glide dislocations with forest dislocations. This has been confirmed by tests on single crystals of aluminum by Mitra, Osborne and Dorn[5] and on polycrystalline aluminum by Mitra and Dorn.[6] Thus in accord with Seeger's theory, the shear strain rate, $\dot{\gamma}$, below a critical temperature, T_c, is

$$\dot{\gamma} = NAb\nu\, e^{-U/kT} \qquad T < T_c \tag{1}$$

where N is the number of points of contact per unit volume between forest dislocations and glide dislocations, A is the area swept out per successful intersection, b is the Burgers vector, ν the frequency of vibration of the segment of the glide dislocation undertaking intersection, U is the activation energy for intersection, k is Boltzmann's constant, and T is the absolute temperature. For aluminum, which has an extremely high stacking fault energy, the constriction energy is negligibly small and therefore the activation energy decreases practically linearly with the stress according to

$$U = U_o \frac{G}{G_o} - \tau^* Lb^2 = U_o \frac{G}{G_o} - (\tau - \tau_{G_o} G/G_o)\, Lb^2, \tag{2}$$

as will be reconfirmed later, where U_o is jog energy at the absolute zero, G and G_o are the shear moduli at the test temperature T and 0°K respectively, L is the spacing of the forest dislocations, τ is the applied shear stress for slip and τ_{G_o} is the stress field that must be surmounted

athermally τ^* being the thermally sensitive component of the stress.† Therefore

$$\tau G_o/G = \tau_{G_o} + \frac{U_o}{Lb^2} - \frac{kTG_o}{Lb^2G} \ln \frac{NAb\nu}{\dot{\gamma}} \quad \text{for } T < T_c \tag{3}$$

where

$$\tau \frac{G_o}{G} = \tau_{G_o} \quad \text{for } T > T_c \tag{4}$$

and

$$\frac{kT_cG_o}{G} \ln \frac{NAb\nu}{\dot{\gamma}} = U_o \tag{5}$$

Since the complete statistical analysis for intersection has not been formulated U_o, τ_{G_o}, L and $NA\nu$ must be taken as appropriately smeared average values.

Although our major interest concerns how τ_{G_o} increases during various types of single and polyslip, we will defer further discussion on this term until later. We will first ascertain how the apparent activation volume, v, for the various types of polyslip depends on the strain, where

$$v = \beta kT = kT \left(\frac{\partial \ln \dot{\gamma}}{\partial \tau} \right)_T = - \left(\frac{\partial U}{\partial \tau} \right)_T \simeq Lb^2 \tag{6}$$

from which L can be determined. Following this we will, by special experiments, evaluate the preexponential coefficient $NAb\nu$ of the Eq. 1 for intersection, and establish the variation of $NAb\nu$ with strain for both polyslip and single slip orientations.

---

† The authors have adopted Conrad's symbols for stresses which differs from the symbols used in Refs. 5 and 6.

III. EXPERIMENTAL TECHNIQUE AND RESULTS

Single crystal bars (3/8" diam) of high purity (99.995 wt.%) aluminum of various orientations were produced under argon by the modified Bridgman technique. Special care was excerised to obtain accurately oriented crystals. The orientations investigated were those for which the tensile axis was in the [001], [011], [$\bar{1}$11], [$\bar{1}$12] and [012] directions plus another for which the Schmid angles for $\{\bar{1}11\}$ <110> slip were $90-\chi_o \simeq \lambda_o = 45 \pm 1°$. A reduced gage section approximately 2" in length and 0.225" in diameter was produced by spark machining. The spark damaged layer was removed by etching away 0.002" from the diameter. Prior to testing, each crystal was annealed at about 828°K in a salt bath for 1/2 hour.

Tests were carried out in an Instron Machine over the temperature range 4.2° to 370°K. Tensile stresses were determined to within $\pm 2 \times 10^6$ dynes/cm^2, tensile strains were measured to within ±0.0001, and the specimen temperature was held to ±0.5°K of the reported values.

An attempt was made to ascertain the number of operative slip systems for each orientation:

45° Only traces of the primary slip plane were observed and the elliptical shape of the deformed crystal clearly revealed that only the primary slip system was operative.

[012] Six specimens exhibited slip only on the primary plane. One-half of one specimen exhibited slip on the primary plane and the other half slip on the critical plane.

[112] This specimen exhibited the commonly reported duplex slip on the principal and conjugate planes. No local necking was observed to take place.

[011] It was difficult to determine accurately from slip line traces alone how many of the four possible slip systems for this orientation were operative. Traces of all four systems were noted but they were difficult to see and were not equally prominent over each section of the crystal. On the other hand, the pole of the tensile axis remained in the [011] direction and the specimen cross section remained circular strongly suggesting that all four possible mechanisms were operative. This deduction coincides with that previously made by Kocks[3] for this orientation.

[111] Slip traces were not sufficiently clear to define the operative number of slip systems. However, the tensile axis remained in the [111] direction and the cross section remained circular. Thus all six possible slip systems are believed to have been operative as previously suggested by Kocks[3] for this orientation.

[001] Whereas the stress strain curve at 77°K differed appreciably from that previously observed by Kocks[3] and by Staubwasser[7] for this orientation at about 300°K, it did agree well with that obtained by Staubwasser at 77°K. Slip traces were not sufficiently distinct to permit identification of the operative slip mechanisms. However, in contrast to specimen tested by Kocks at 300°K, this specimen remained circular in cross section and the pole of the tensile axis remained in the [001] direction. These factors suggest that eight slip systems were operative. Furthermore,

the stress strain curve, to be described later, also suggests that eight possible systems were operative. Although it is not immediately apparent as to why this specimen differed in operative slip systems from that described by Kocks, it is possible that this difference is ascribable either to the difference in test temperature or differences in variations from the ideal orientation.

The tensile stress strain diagrams that were obtained are in nominal agreement with those previously determined by Staubwasser[7] at 77°K. To facilitate analyses, the original data were converted into the resolved shear stress τ resolved shear strain γ, diagrams given in Fig. 1, because they are directly analysed relative to the nature of strain hardening. The significant resolved shear stresses and shear strains are those on any one of the several equivalent operative slip systems during polyslip. Such diagrams have the virtue of describing the shear stress-shear strain diagram for slip on any one plane when other systems are also operating during polyslip. The conversions that were used are given in Appendix A and summarized in Table I.

As shown in Fig. 1, the initial yield stress was independent of crystal orientation. Furthermore, the consistency of these data attest to the fact that the initial dislocation patterns were quite similar for the various specimens. None of the specimens exhibited much easy glide and all appeared to enter the linear hardening region of Stage II early in the deformation. Two significant facts are revealed: First, the rate of linear hardening of Stage II increases as the number of operative slip systems increase. And secondly, the initiation of Stage III takes place at

TABLE I

Resolved Shear Strains and Shear Stresses
on a Single Operative Slip Plane

Case	Tensile Axis	Typical Operative Slip: Direction	Typical Operative Slip: Plane Normal	$\cos\lambda_o$	$\sin\chi_o$	No. Slips n	General Shear Strain γ	General Shear Stress τ	Shear Strain γ	Shear Stress τ
A	45°	$[\bar{1}01]$	[111]	$1/\sqrt{2}$	$1/\sqrt{2}$	1	$\dfrac{\sqrt{\left(\ell/\ell_o\right)^2-\sin^2\lambda_o}-\cos\lambda_o}{\sin\chi_o}$	$\dfrac{L}{A_o}\sin\chi_o\sqrt{1-\left(\dfrac{\ell_o}{\ell}\right)^2\sin^2\lambda_o}$	$\sqrt{2\left(\dfrac{\ell}{\ell_o}\right)^2-1}-1$	$L/A_o\sqrt{\dfrac{1}{2}-\dfrac{1}{4}\left(\dfrac{\ell_o}{\ell}\right)^2}$
B	[012]			$\sqrt{2/5}$	$\sqrt{3/5}$	1	"	"	$\sqrt{5/3\left(\dfrac{\ell}{\ell_o}\right)^2-1}-\sqrt{2/3}$	$L/A_o\sqrt{\dfrac{3}{5}\left\{1-\left(\dfrac{\ell_o}{\ell}\right)^2\dfrac{3}{5}\right\}}$
C	$[\bar{1}12]$			$\sqrt{3}/2$	$\sqrt{2}/3$	2	$\dfrac{\ell n\,\ell/\ell_o}{n\cos\lambda_o\sin\chi_o}$	$\dfrac{L}{A_o}\dfrac{\ell}{\ell_o}\sin\chi_o\cos\lambda_o$	$\sqrt{\dfrac{6}{2}}\,\ell n\,\ell/\ell_o$	$L/A_o\left(\dfrac{\ell}{\ell_o}\right)\sqrt{\dfrac{1}{6}}$
D	[011]			1/2	$\sqrt{2/3}$	4	"	"	$\sqrt{\dfrac{6}{4}}\,\ell n\,\ell/\ell_o$	$L/A_o\left(\dfrac{\ell}{\ell_o}\right)\sqrt{\dfrac{1}{6}}$
E	$[\bar{1}11]$			$\sqrt{2/3}$	1/3	6	"	"	$\sqrt{\dfrac{6}{4}}\,\ell n\,\ell/\ell_o$	$L/A_o\left(\dfrac{\ell}{\ell_o}\right)\sqrt{\dfrac{2}{27}}$
F	[001]			$1/\sqrt{2}$	$1/\sqrt{3}$	8	"	"	$\sqrt{\dfrac{6}{8}}\,\ell n\,\ell/\ell_o$	$L/A_o\left(\dfrac{\ell}{\ell_o}\right)\dfrac{1}{\sqrt{6}}$

ℓ and ℓ_o are the instantaneous and initial gage lengths, A_o is the initial cross sectional areas, λ_o and χ_o are the initial Schmid angles, and n is the number of equivalent operative slip systems

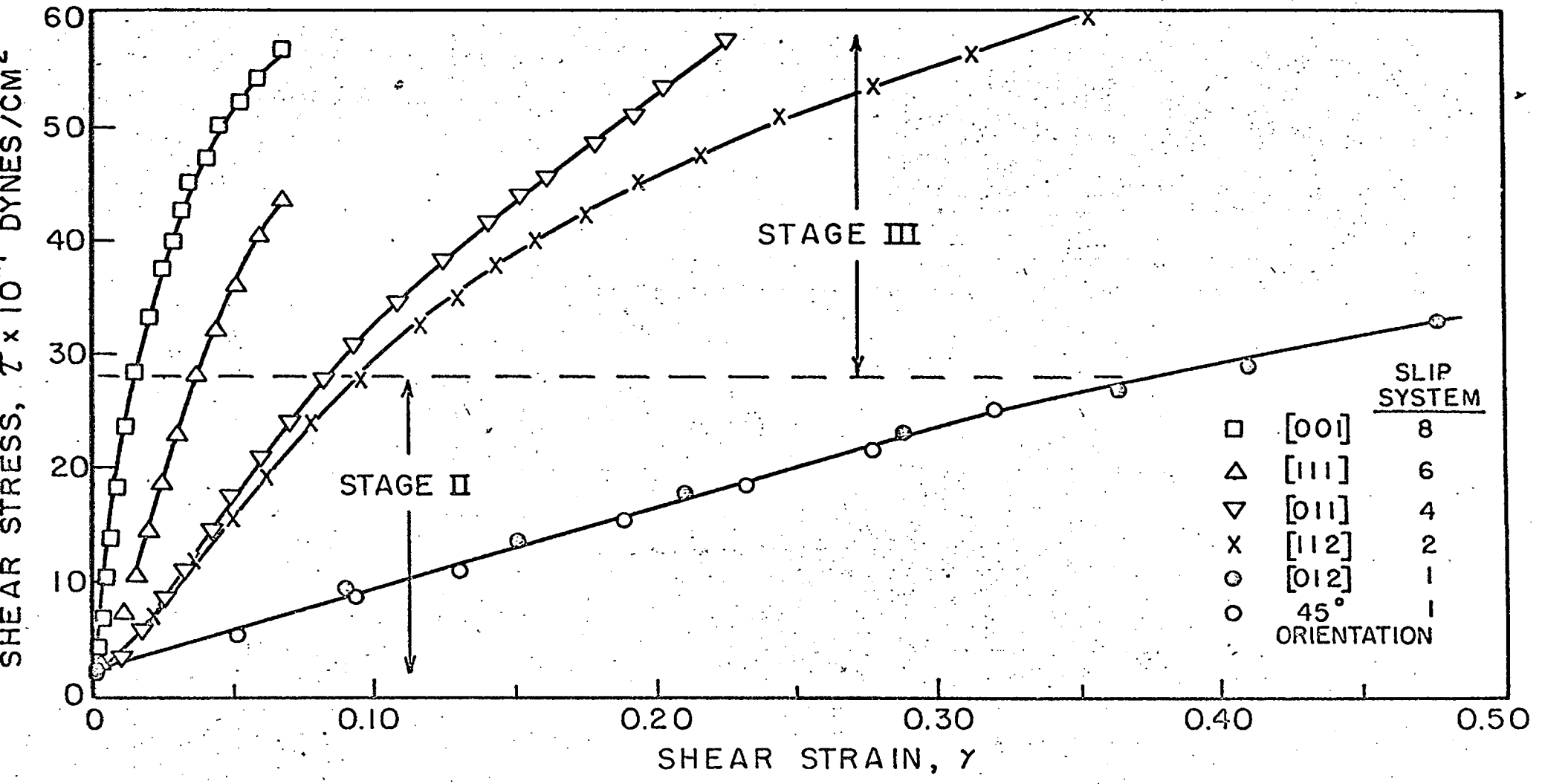
SHEAR STRESS, $\tau \times 10^{-4}$ DYNES/CM^2
60
50
40
30
20
10
0
0
0.10
0.20
0.30
0.40
0.50
SHEAR STRAIN, γ
STAGE II
STAGE III
SLIP SYSTEM
[001] 8
[111] 6
[011] 4
[112] 2
[012] 1
45° ORIENTATION 1

FIG. 1.

about the same stress level regardless of the number of operative slip systems. Therefore, Stage III starts at lower strains as the number of operative slip systems is increased. As noted by Kocks,[3] these issues are significant to the formulation of the theory for work hardening in polycrystalline aggregates.

Auxiliary tests involving a change in strain rate by a factor of ten were employed to measure β (Eq. 6) from which the apparent activation volume was deduced. The resulting data, given in Fig. 2, reveal that the apparent activation volume for each orientation decreases with increasing strain. The rate at which this happens increases with the number of operative slip systems. This reveals that the mean spacing L of the forest dislocations decreases more rapidly with strain hardening the greater the amount of polyslip. When these data are replotted as shown in Fig. 3, it is seen that the flow stress τ increases linearly with the reciprocal of the activation volume and therefore the reciprocal of L. The lines for the various orientations converge to a single point at about $\tau \simeq 1.5 \times 10^7$ dynes/cm^2 and $1/v \simeq 0.27 \times 10^{-21}$ 1/cm^3, implying that the density of the forest dislocations was about the same for all orientations at the initial yield strength. The linear increase in τ with $1/\beta kT$, however, increased systematically with the number of operative slip systems. It is therefore clear that the activation volume is not the only factor responsible for strain hardening, for, if it were, the lines for the various orientations would have coincided. Consequently, a second factor, to be identified later, as the stress fields τ_G, that must be surmounted athermally, also increase with increasing amounts of polyslip.

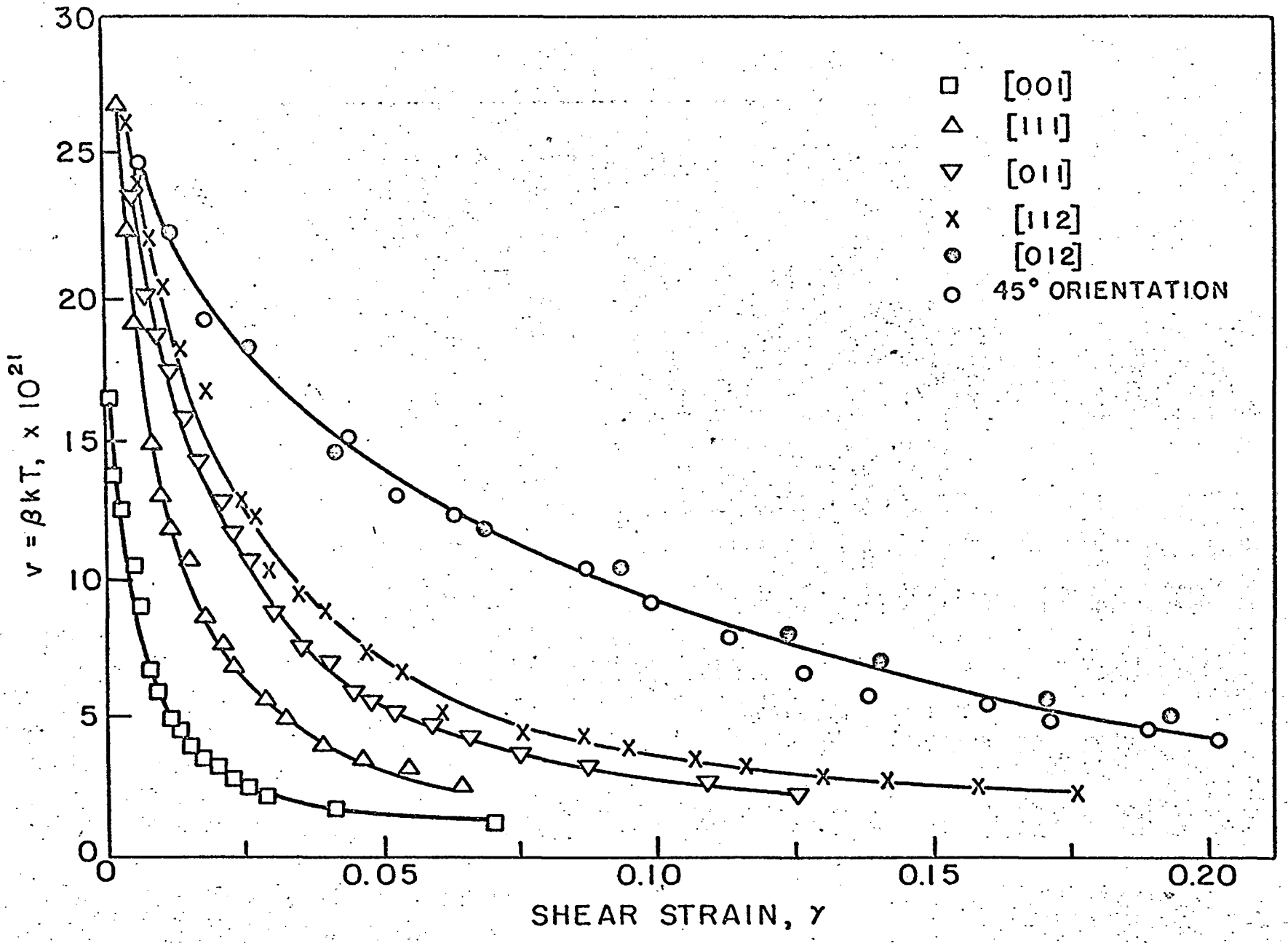

FIG. 2 ACTIVATION VOLUME vs. SHEAR STRAIN.

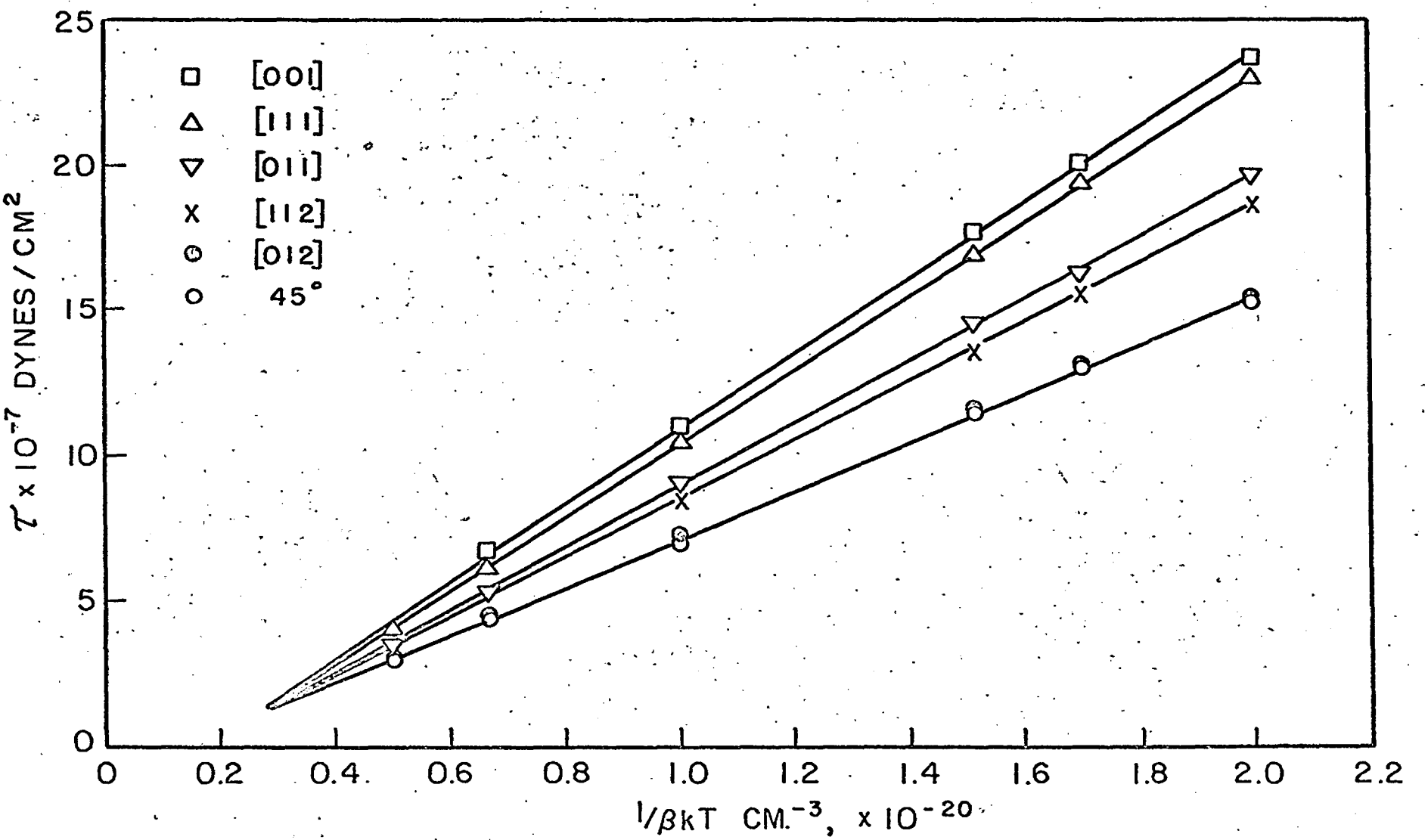

FIG. 3 VARIATION OF τ WITH $1/\beta kT$ FOR DIFFERENT ORIENTATIONS.

In addition to the activation volume v, discussed above, two other factors inherent in the intersection model, namely, $NAb\nu$ and τ_G, might also depend on the strain-hardened state. Special tests were made to ascertain how $NAb\nu$ might be affected by straining for several orientations, namely the [111] orientation which had six operative slip systems and the $\chi_o = \lambda_o = 45°$ orientation which exhibited only one prominent slip system. For this purpose, a series of crystals of each orientation were prestrained at 370°K and a tensile strain rate of 1.0×10^{-5} per sec to various strain-hardened states designated as a, b, etc. Each specimen was prestrained to the lowest state (a) prescribed by the flow stress τ_P for the prestrain temperature and strain rate, subsequently deformed at the selected temperature and strain rate, returned to the prestrain temperature and prestrained to state (b) etc. By this procedure errors arising from sepcimen variations were substantially reduced.

The data so obtained over Region I, recorded in Figs. 4 and 5, are in good agreement with the dictates of Eq. 3 for the intersection model. Over Region II for the lowest strain-hardened states, the data also correspond well with the theory (Eq. 4). On the other hand, the higher strain hardened states exhibited a slightly decreasing value of $\tau G_o/G$ with increasing temperature and decreasing strain rate suggesting that for these states a minor amount of a thermally activated-stress assisted mechanism is superimposed on the athermal behavior.

The value of $\ell n\, NAb\nu$ for each strain-hardened state can be deduced from the slopes of the curves of Figs. 4 and 5 over Region I for the two strain rates. As shown by Eq. 3

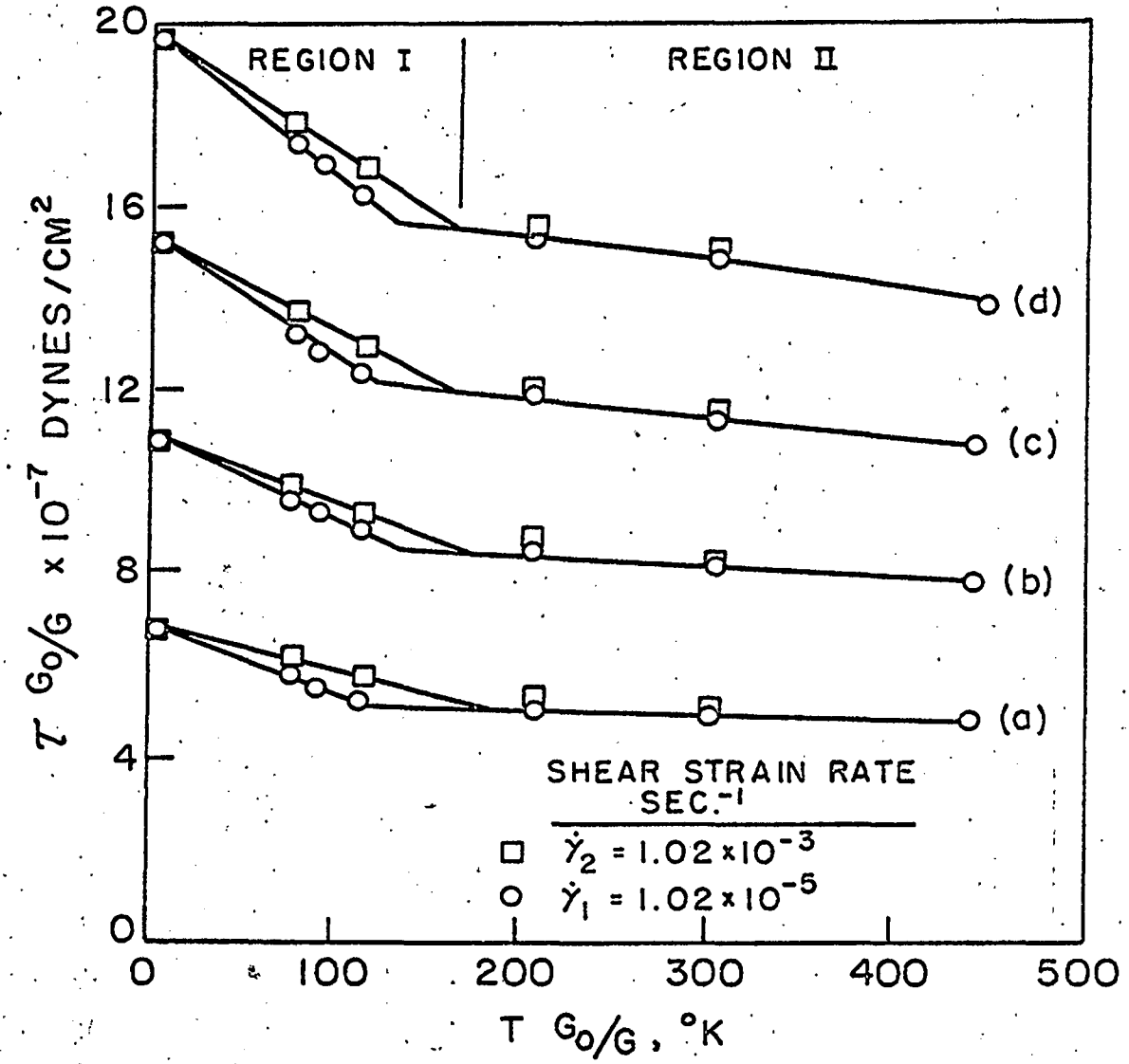

FIG. 4 EFFECT OF TEMPERATURE ON THE FLOW STRESS. [111] ORIENTATION.

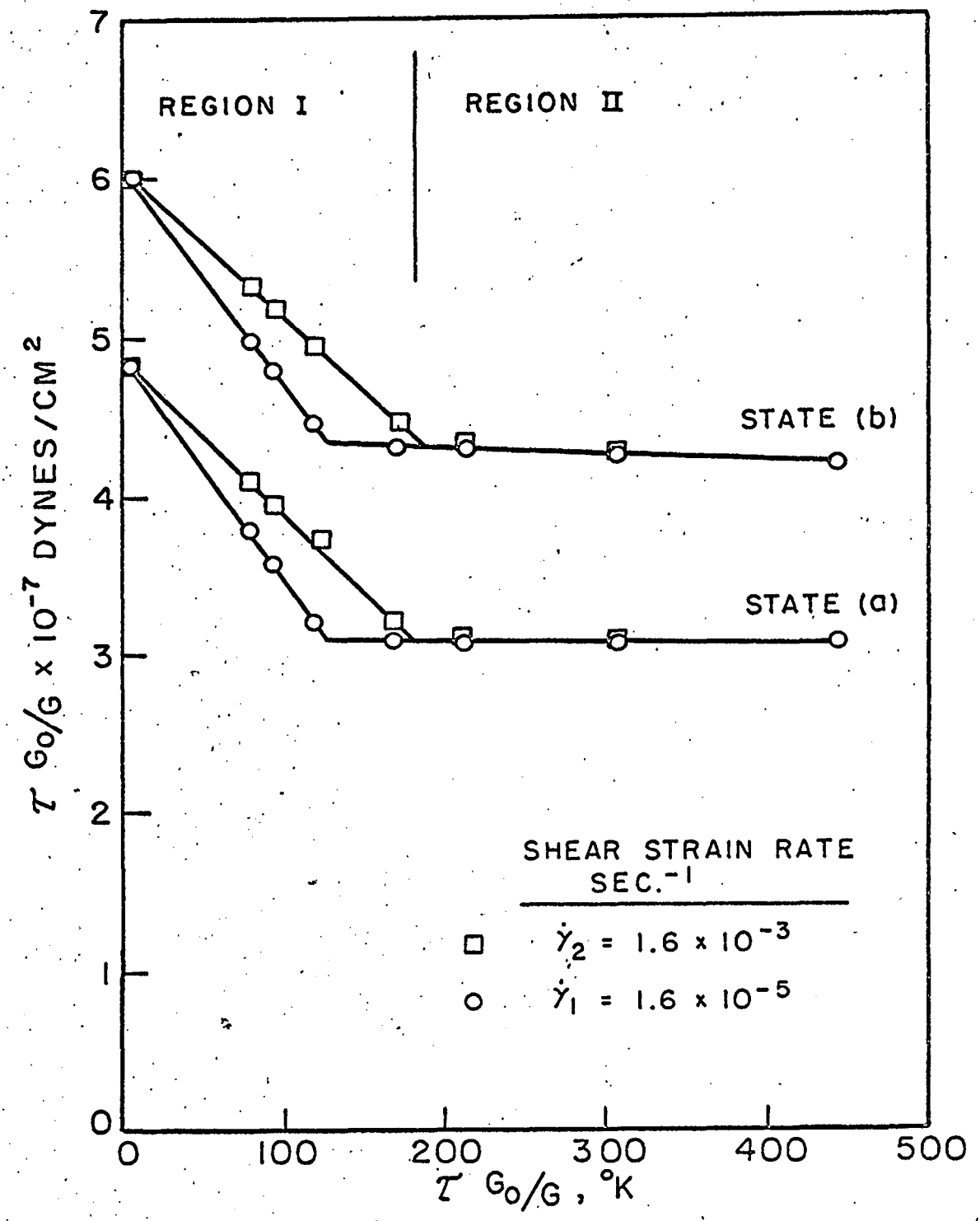

FIG. 5 EFFECT OF TEMPERATURE AND STRAIN RATE ON THE FLOW STRESS. 45° ORIENTATION.

$$S = \frac{\partial \tau G_o/G}{\partial T} = \frac{-k}{Lb^2} \frac{G_o}{G} \left\{ \ell n(NAb\nu) - \ell n \dot{\gamma} \right\} \tag{7}$$

and therefore

$$\frac{S_2}{S_1} = \frac{\ell n(NAb\nu) - \ell n \dot{\gamma}_2}{\ell n(NAb\nu) - \ell n \dot{\gamma}_1} \tag{8}$$

from which $\ell n(NAb\nu)$ was obtained. The experimentally deduced values, given in Table II, reveal that $NAb\nu$ increases with strain hardening.

Various correlations of $NAb\nu$ with the strain hardened state were attempted, the most revealing being that given in Fig. 6 where $NAb\nu$ is compared with the activation volume Lb^2. In addition to the data determined here, other previously reported data, namely that deduced from experiments by Mitra, Osborne and Dorn[5] on single crystals of Al and that given by Nunes, Rosen and Dorn[8] on polycrystalline Al, have also been incorporated in the figure. The sum total of these correlations strongly imply that $NAb\nu$ increases over the range that was investigated in a way that parallels the increase in the reciprocal of the activation volume with strain hardening. Since the same correlation is obtained for a single slip system, six slip systems and polyslip in polycrystalline aggregates, it is insensitive to the number of operative slip systems.

The total activation energy for intersection was determined from the effect of strain rate on T_c. Equation 5 can be written as

$$\dot{\gamma}_2/\dot{\gamma}_1 = \frac{e^{-(U_o G/G_o)/kT_{c_2}}}{e^{-(U_o G/G_o)/kT_{c_1}}} \tag{9}$$

From Figs. 4 and 5, using T_{c_2} and T_{c_1} for state (a), one can calculate the total activation energy for intersection U_o. The value for the activation

TABLE II

Variation of NAbν with State

State	$\tau_p G_o / G \times 10^7$ dynes/cm^2	NAbν sec^{-1}
[111] orientation		
(a)	4.81	2.0×10^3
(b)	7.82	2.3×10^5
(c)	10.69	5.8×10^7
(d)	13.89	7.6×10^8
45° orientation		
(a)	3.05	6.69×10^3
(b)	4.2	1.01×10^6

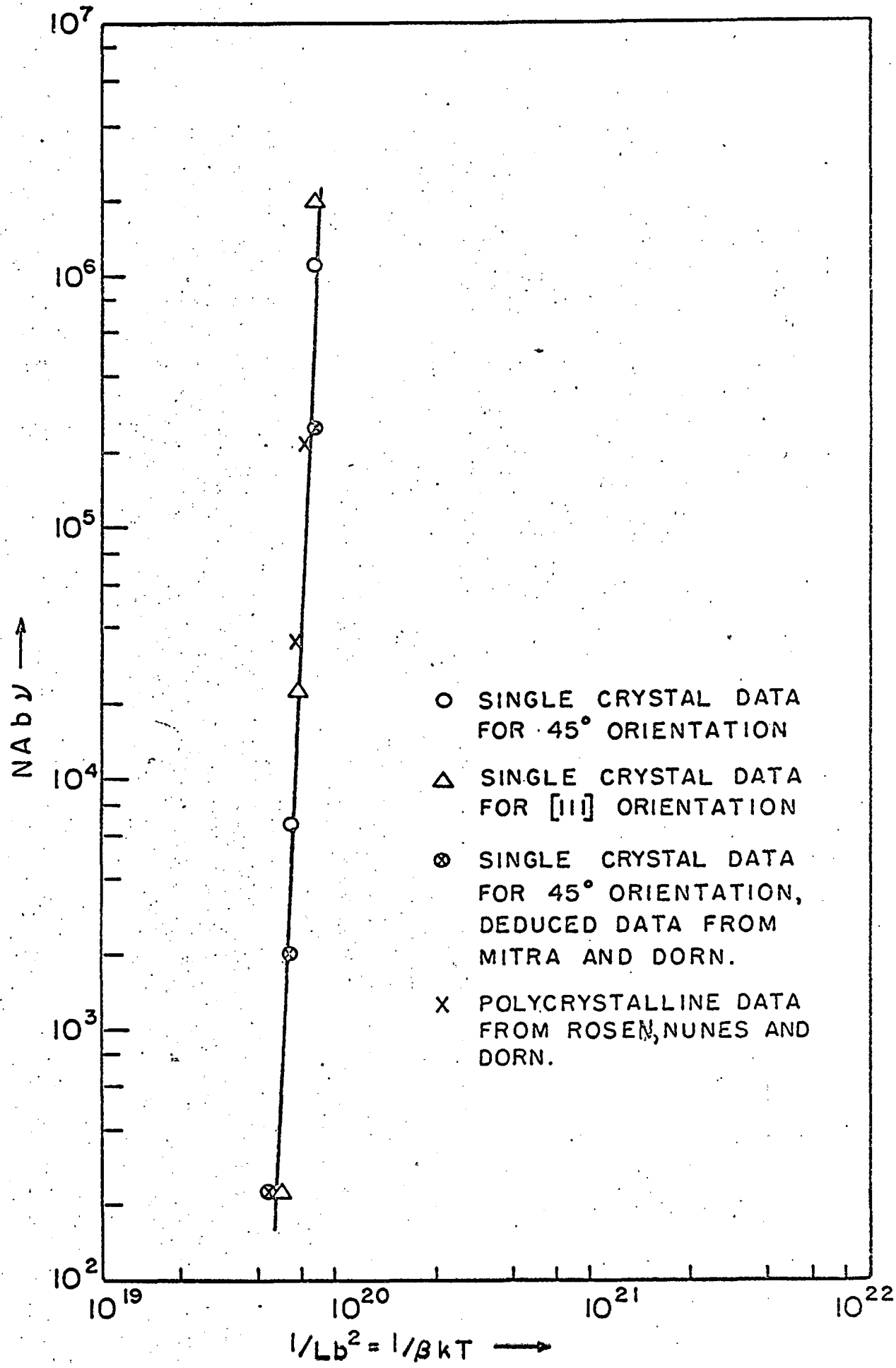
10^7
10^6
10^5
10^4
10^3
10^2
$NAbv \longrightarrow$
10^{19}
10^{20}
10^{21}
10^{22}
$1/Lb^2 = 1/\beta kT \longrightarrow$
O SINGLE CRYSTAL DATA FOR 45° ORIENTATION
△ SINGLE CRYSTAL DATA FOR [111] ORIENTATION
⊗ SINGLE CRYSTAL DATA FOR 45° ORIENTATION, DEDUCED DATA FROM MITRA AND DORN.
X POLYCRYSTALLINE DATA FROM ROSEN, NUNES AND DORN.

FIG. 6

energy is U_o = 4,400cal/mole for the [111] orientation crystals and 4,200cal/mole for the 45° orientation crystals. These values of U_o compare favorably with that of 4,700cal/mole obtained by Rosen, Nunes and Dorn[8] for polycrystalline Al. Thus, the average value of the activation energy for intersection is $U_o \simeq 0.05 G_o b^3$ and it is somewhat lower than the crude estimated value[9] of $0.08 G_o b^3$ for the formation of a single jog in essentially undissociated dislocations.

The value of τ_G for the 77°K data can now be deduced using Eq. 3 from the data recorded in Figs. 1, 2, 3 and 6 and the now known value of U_o. The variation of τ_{G_o} with $1/Lb^2$ obtained by these correlations is given in Fig. 7. Thus τ_{G_o} increases about linearly with $1/Lb^2$ and the rate of increase is greater for higher amounts of polyslip.

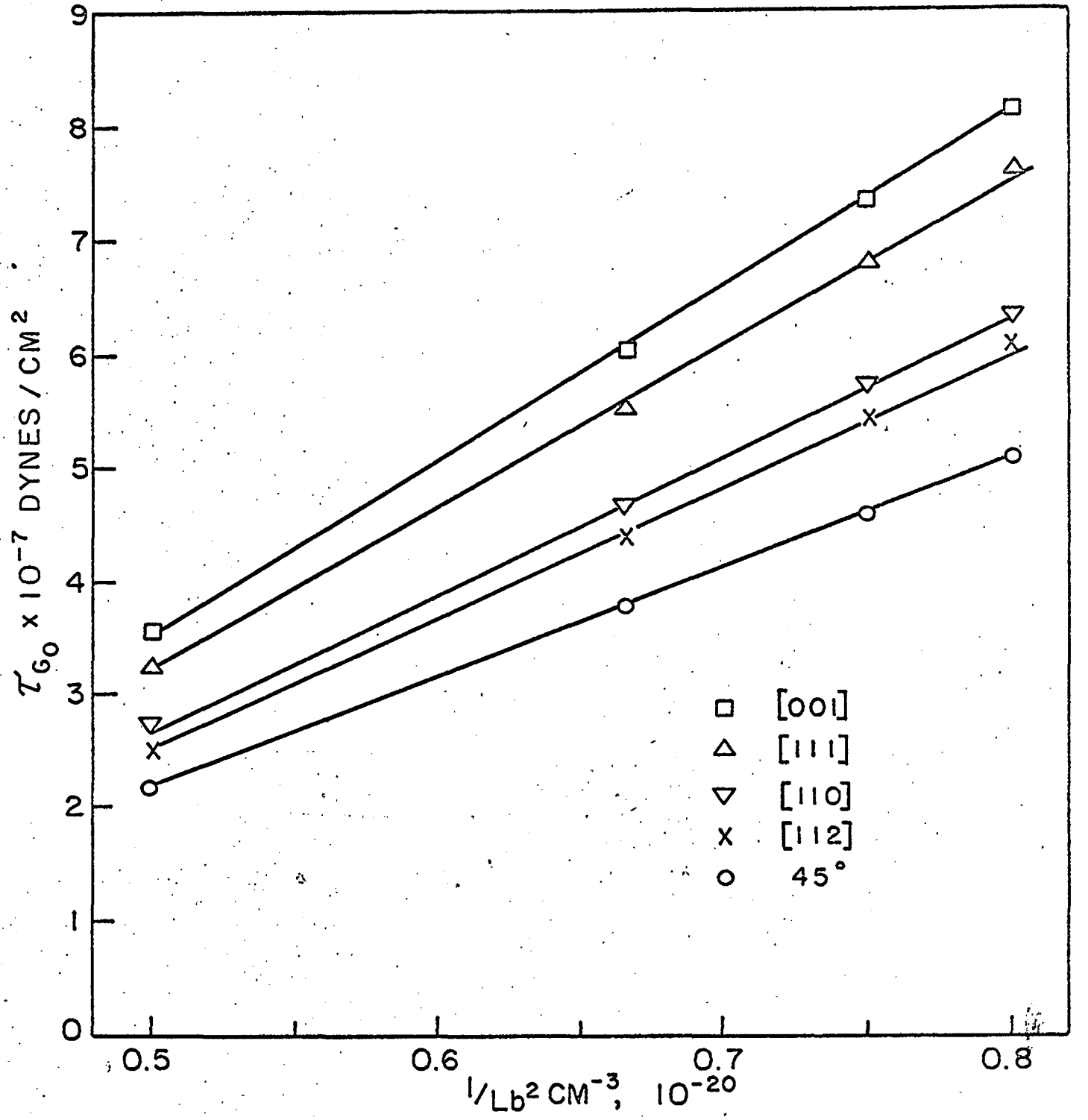

FIG. 7 VARIATION OF τ_{G_0} WITH $1/Lb^2$ FOR DIFFERENT ORIENTATIONS.

IV. DISCUSSION

Over the past twenty years a number of suggestions have been made on possible models for strain hardening.[1, 10-14] Although limitations on space prohibit a review of this subject here, it is necessary to record that strain hardening is a complicated phenomenon which undoubtedly arises from the superposition of a series of effects. It is therefore highly unlikely that any single investigation, such as that made here, will completely rationalize strain hardening in all of its details. Nevertheless, the present data appear to reveal one of the major factors involved in the dislocation mechanics of strain hardening.

Several models for strain hardening are based on the concept that the slipping dislocations interact with some dislocations of the network to produce low energy configurations which then restrain motion of the slipping dislocations in their vicinity. According to this concept the greatest rate of strain hardening during polyslip should occur when polyslip leads to the greatest number of stable dislocation configurations.

Whereas dislocation reactions during single slip occur between the essentially stable network and the slip dislocations, under polyslip more rapid formation of stable configurations can arise as a result of reactions between the sets of slipping dislocations on the several operative slip planes. An evaluation of the interactions between such sets of slip dislocations is given in Table III in terms of the interaction energies. In this evaluation only large factors are considered; the minor variations arising from a more detailed description which takes forces and torques into consideration and distinctions between edge and screw dislocations

impose only minor variations on the following deductions. Furthermore, the omission of considerations of anisotropy and the dissociation of dislocations into their partials is not serious for the case of Al being considered here.

The stable attractive reactions for the 45° and [012] orientations arise exclusively from interactions between the glide dislocations and those in the dislocation network. Consequently, the rate of strain hardening for these two orientations is the same and small. In contrast, the slip dislocations for a crystal in the $[\bar{1}12]$ orientation can form a single low energy combination, recorded in Table III, which lies, as shown in Fig. 8a, along the $[1\bar{1}0]$ direction; a greater rate of strain hardening is therefore expected than that obtained during single slip. For the [011] orientation, two dislocation reactions result in low energy configurations where the resultant dislocations have the same Burger's vector and lie in the $[0\bar{1}1]$ direction (vide Fig. 8b). Three sets of reactions leading to a reduction of energy take place between the various glide dislocations for crystals having the $[\bar{1}11]$ orientation; their arrangement on each slip plane is illustrated in Fig. 8c. Slip dislocations in crystals having the [001] orientation undergo four stabilizing reactions (vide Table III) resulting in the stable dislocations shown in Fig. 8d. Thus there is good qualitative agreement between the experimentally determined rates of strain hardening and the number of geometric disposition of attractive combinations of slip dislocations during various degrees of polyslip.

Either Lomer-Cottrell[15,16] barriers or the formation of attractive junctions as described by Saada[4] could account for the correlations

TABLE III

Orientation	Slip Systems	Significant Interactions	$\Delta U/a^2$	No. of attractive barriers
45°	$(111)[\bar{1}01]$	none		
[012]	$(111)[\bar{1}01]$	none		
$[\bar{1}12]$	$(111)[\bar{1}01]$	$1/2a[\bar{1}01]+1/2a[011] \rightarrow \pm 1/2a[\bar{1}12]$	+1/2	1
	$(\bar{1}\bar{1}1)[011]$	$1/2a[\bar{1}01]+1/2a[0\bar{1}\bar{1}] \rightarrow \pm 1/2a[\bar{1}\bar{1}0]$	-1/2	
{011}	$(111)[\bar{1}01]$	$1/2a[\bar{1}01]+1/2a[101] \rightarrow \pm 1/2a[002]$	0	
	$(111)[1\bar{1}0]$	$1/2a[\bar{1}01]+1/2a[\bar{1}0\bar{1}] \rightarrow \pm 1/2a[\bar{2}00]$	0	
	$(\bar{1}11)[101]$	$1/2a[\bar{1}01]+1/2a[110] \rightarrow \pm 1/2a[011]$	-1/2	
	$(\bar{1}11)[110]$	$1/2a[\bar{1}01]+1/2a[\bar{1}\bar{1}0] \rightarrow \pm 1/2a[\bar{2}\bar{1}1]$	+1/2	
		$1/2a[1\bar{1}0]+1/2a[101] \rightarrow \pm 1/2a[2\bar{1}1]$	+1/2	
		$1/2a[1\bar{1}0]+1/2a[\bar{1}0\bar{1}] \rightarrow \pm 1/2a[0\bar{1}\bar{1}]$	-1/2	
		$1/2a[1\bar{1}0]+1/2a[110] \rightarrow \pm 1/2a[200]$	0	
		$1/2a[1\bar{1}0]+1/2a[\bar{1}\bar{1}0] \rightarrow \pm 1/2a[0\bar{2}0]$	0	
$[\bar{1}11]$	$(111)[\bar{1}01]$	$1/2a[\bar{1}01]+1/2a[011] \rightarrow \pm 1/2a[\bar{1}12]$	+1/2	
	$(111)[1\bar{1}0]$	$1/2a[\bar{1}01]+1/2a[0\bar{1}\bar{1}] \rightarrow \pm 1/2a[\bar{1}\bar{1}0]$	-1/2	
	$(\bar{1}\bar{1}1)[011]$	$1/2a[\bar{1}01]+1/2a[1\bar{1}0] \rightarrow \pm 1/2a[0\bar{1}1]$	-1/2	3
	$(\bar{1}\bar{1}1)[1\bar{1}0]$	$1/2a[\bar{1}01]+1/2a[\bar{1}10] \rightarrow \pm 1/2a[\bar{2}11]$	+1/2	
	$(1\bar{1}1)[011]$	$1/2a[1\bar{1}0]+1/2a[011] \rightarrow \pm 1/2a[101]$	-1/2	
	$(1\bar{1}1)[\bar{1}01]$	$1/2a[1\bar{1}0]+1/2a[0\bar{1}\bar{1}] \rightarrow \pm 1/2a[1\bar{2}\bar{1}]$	+1/2	
		$1/2a[\bar{1}01]+1/2a[\bar{1}01] \rightarrow \pm 1/2a[\bar{2}02]$	+1	

TABLE III (Continued)

Orientation	Slip Systems	Significant Interactions	$\Delta U/a^2$	No. of attractive junctions
		$1/2a[\bar{1}01]+1/2a[10\bar{1}] \rightarrow \pm 1/2a[000]$	annhilation	
		$1/2a[1\bar{1}0]+1/2a[1\bar{1}0] \rightarrow \pm 1/2a[2\bar{2}0]$	+1	
		$1/2a[1\bar{1}0]+1/2a[\bar{1}10] \rightarrow \pm 1/2a[000]$	annhilation	
		$1/2a[011]+1/2a[011] \rightarrow \pm 1/2a[022]$	+1	
		$1/2a[011]+1/2a[0\bar{1}\bar{1}] \rightarrow \pm 1/2a[000]$	annhilation	
[001]	$(111)[\bar{1}01]$	$1/2a[\bar{1}01]+1/2a[011] \rightarrow \pm 1/2a[\bar{1}12]$	+1/2	
	$(111)[0\bar{1}1]$	$1/2a[\bar{1}01]+1/2a[0\bar{1}\bar{1}] \rightarrow \pm 1/2a[\bar{1}\bar{1}0]$	-1/2	
	$(\bar{1}\bar{1}1)[011]$	$1/2a[\bar{1}01]+1/2a[101] \rightarrow \pm 1/2a[002]$	0	
	$(\bar{1}\bar{1}1)[101]$	$1/2a[\bar{1}01]+1/2a[\bar{1}0\bar{1}] \rightarrow \pm 1/2a[\bar{2}00]$	0	
	$(1\bar{1}1)[011]$	$1/2a[\bar{1}01]+1/2a[0\bar{1}1] \rightarrow \pm 1/2a[\bar{1}\bar{1}2]$	+1/2	
	$(1\bar{1}1)[\bar{1}01]$	$1/2a[\bar{1}01]+1/2a[01\bar{1}] \rightarrow \pm 1/2a[\bar{1}10]$	-1/2	4
	$(\bar{1}11)[101]$	$1/2a[0\bar{1}1]+1/2a[011] \rightarrow \pm 1/2a[002]$	0	
	$(\bar{1}11)[0\bar{1}1]$	$1/2a[0\bar{1}1]+1/2a[0\bar{1}\bar{1}] \rightarrow \pm 1/2a[0\bar{2}0]$	0	
		$1/2a[0\bar{1}1]+1/2a[101] \rightarrow \pm 1/2a[1\bar{1}2]$	+1/2	
		$1/2a[0\bar{1}1]+1/2a[\bar{1}0\bar{1}] \rightarrow \pm 1/2a[\bar{1}\bar{1}0]$	-1/2	
		$1/2a[011]+1/2a[101] \rightarrow \pm 1/2a[112]$	+1/2	
		$1/2a[011]+1/2a[\bar{1}0\bar{1}] \rightarrow \pm 1/2a[\bar{1}10]$	-1/2	
		$1/2a[\bar{1}01]+1/2a[\bar{1}01] \rightarrow \pm 1/2a[\bar{2}0\bar{2}]$	+1	
		$1/2a[\bar{1}01]+1/2a[10\bar{1}] \rightarrow \pm 1/2a[000]$	annhilation	
		$1/2a[0\bar{1}1]+1/2a[0\bar{1}1] \rightarrow \pm 1/2a[0\bar{2}2]$	+1	
		$1/2a[0\bar{1}1]+1/2a[01\bar{1}] \rightarrow \pm 1/2a[000]$	annhilation	

TABLE III (Continued)

Orientation	Slip Systems	Significant Interactions	$\Delta U/a^2$	No. of attractive junctions
		$1/2a[011]+1/2a[011] \rightarrow \pm 1/2a[022]$	+1	
		$1/2a[011]+1/2a[0\bar{1}\bar{1}] \rightarrow \pm 1/2a[000]$	annhilation	
		$1/2a[101]+1/2a[101] \rightarrow \pm 1/2a[202]$	+1	
		$1/2a[101]+1/2a[\bar{1}0\bar{1}] \rightarrow \pm 1/2a[000]$	annhilation	

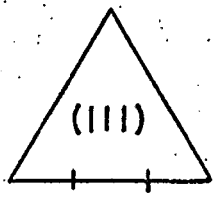

(a) $[\bar{1}12]$ ORIENTATION. BARRIER PARALLEL TO $[1\bar{1}0]$

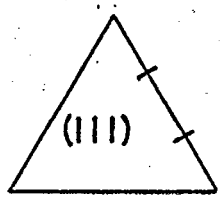

(b) $[011]$ ORIENTATION. BARRIER PARALLEL TO $[0\bar{1}1]$

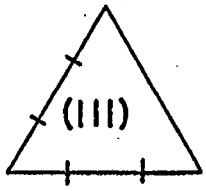

(c) $[\bar{1}11]$ ORIENTATION. BARRIER PARALLEL TO $[10\bar{1}]$ AND $[1\bar{1}0]$

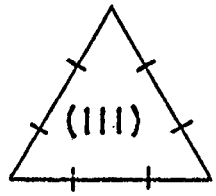

(d) $[001]$ ORIENTATION BARRIER PARALLEL TO $[1\bar{1}0]$, $[10\bar{1}]$ AND $[0\bar{1}1]$

FIG. 8

discussed above. Seeger[1] suggested that the linear (Stage II) strain hardening in FCC crystals results from pile-up arrays of dislocations restrained by Lomer-Cottrell locks. Although Lomer-Cottrell barriers are observed[17] in low stacking fault metals or alloys, there is no evidence of the formation of these barriers in Al. On the contrary, a cell structure bounded by dense dislocation tangles is formed.[18] Hirsch[19] and Kuhlmann-Wilsdorf[14] have offered other substantial objections to the operation of the Seeger mechanism in high stacking fault metals.

Hirsch[19] first observed that attractive junctions frequently formed between moving dislocations and the forest dislocations. These reactions, which are promoted by the same type of reactions that lead to the formation of Lomer-Cottrell dislocations have been studied in detail by Saada.[4] He made the following simplifying assumptions:

1. The trees are inflexible.
2. The junction dislocation remains immobile.
3. The Burger's vectors are all equal in magnitude and make angles of 120° with each other.
4. The moving dislocation is flexible and has a line tension of about $Gb^2/2$.
5. The dislocations are undissociated.

Assumptions, 1, 2, and 4 are not serious and assumption 3 limits the analysis to FCC crystals. Furthermore, assumption 5 is very good for Al.

Saada demonstrated that the energy required for dislocations to cut through repulsive junctions was small. Such intersections undoubtedly account for the thermally sensitive stress $\tau - \tau_G$ for intersection. He

found that the stresses required to cut through attractive junctions were much higher than those needed to overcome the long range back stresses of the network of dislocations. On this basis, he suggested that the athermal stress τ_G arises largely from cutting attractive junctions whence

$$\tau_G = \frac{Gb}{BL_A}$$

where L_A = the mean distance between attractive junctions ($L_A \simeq 2L$)

$B \simeq 2.5$

The correlation between Saada's theory and the previously deduced experimental results, as given by the example in Table IV, is excellent.

Thin foil electron microscopy of both single and polycrystalline Al has shown evidence of extensive dislocation tangling[18] even at the smallest deformations yet investigated. Cross slip[1] has been suggested as the possible cause of tangling. The main argument against cross slip as a dominant mechanism for dislocation tangling is that entanglement is known to occur even at the lowest strains of Stage I and Stage II whereas extensive cross-slip does not set in before the beginning of Stage III. Cross slip could conceivably contribute to the process of entanglement and cell formation in Stage III but it cannot be the sole mechanism for their formation.

An alternate concept that interactions between point defects and dislocations are basically responsible for tangling was proposed by Kuhlmann-Wilsdorf.[20] The process of intersection of dislocations itself is a source for the production of point defects. Saada has shown[4] that the cutting of an attractive tree is a dynamical process and the kinetic energy

TABLE IV

State	βkT at 77°K $\times 10^{-20} cm^3$	$L = \frac{\beta kT}{b^2}$ $\times 10^{-5} cm$	$\tau_G = \frac{Gb}{2BL}$ $\times 10^7 dynes/cm^2$	τ_G experimental at 77°K $\times 10^7 dynes/cm^2$
(a)	2.4	2.934	5.3	5.02
(b)	1.6	1.95	8.01	8.19

released is sufficient for the production of point defects. Furthermore, Friedel (see Ref. 9 page 274) has shown that at low and intermediate temperatures the point defect concentration due to such a process results in a very high supersaturation even after small strains. Consequently point defects will condense and be annihilated at sinks, causing dislocations to climb and thus to be deflected out of their slip planes. Since such climb does not take place uniformly, the glide motion of the dislocations will be blocked in certain places. Thus various complicated processes might contribute to the formation of entanglements.

CONCLUSIONS

1. The experimental results confirm that the rate controlling mechanism of deformation of aluminum at low temperatures is one of intersection of dislocations.
2. The preexponential coefficient of the Seeger equation for intersection is not constant during deformation as has been previously assumed but changes by several orders of magnitude. The preexponential coefficient increased over the range that was investigated in a way that parallels the increase in the reciprocal of the activation volume with strain hardening. Since the same correlation was obtained for single slip and polyslip systems, the coefficient was insensitive to the number of operative slip systems.
3. The activation volume decreased more rapidly with deformation as the number of operative slip systems increased.
4. The rate of strain hardening increased for those orientations wherein attractive dislocation interactions could occur and that those orientations which produced the greater number of such attractive intersections exhibited the greater strain hardening.
5. The deformation of the region above the critical temperature for the higher strain hardened states, showed a minor amount of a thermally-activated stress-assisted mechanism, that was superimposed on the athermal behavior.
6. Entanglements undoubtedly play a role in the theory of strain hardening. Saada's theory merely relates the athermal flow stress to the density of dislocations. It seems likely that the formation of entanglements will account for the linear rate of strain hardening that is observed over Stage II.

ACKNOWLEDGMENTS

This research was conducted as part of the activities of the Inorganic Materials Research Division of the Lawrence Radiation Laboratory of the University of California, Berkeley. The authors express their appreciation to the United States Atomic Energy Commission for their support of this effort. Thanks are also due Mr. R. Walson and Mr. G. Chao for the assistance in growing the aluminum single crystals.

REFERENCES

1. A. Seeger, "The Mechanism of Glide and Work Hardening in F. C. C. and H. C. P. Metals," Dislocation and Mechanical Properties of Crystals (John Wiley and Sons, New York, 1956) pp. 243-332.
2. L. M. Clareborough and M. E. Hargreaves, "Work Hardening of Metals," Progress in Metal Physics (Pergamon Press, 1959) Vol. 8, pp. 1-103.
3. U. F, Kocks, "Polyslip in Single Crystals," Acta Met., 8, 345-352 (1960).
4. G. Saada, "Sur L'Interaction d'une Dislocation Fixe et d'une Dislocation Mobile Dans Son Plan de Glissement," Acta Met., 8, 200-208 (1960); "Sur le Durcissement du a la Recombinaison des Dislocations," Acta. Met., 8, 841-847 (1960); "Interaction de Dislocation, Ecrouissage et Production de Defauts Ponctuels dans less Metaux c.f.c., Acta Met., 9, 166 (1961); Acta Met., 10, 551 (1962); "Dislocations Interactions and Plastic Deformation of Crystals," Electron Microscopy and Strength of Crystals, (Interscience Publishers, 1963) pp. 651-660.
5. S. K. Mitra, P. W. Osborne and J. E. Dorn, "On the Intersection Mechanism of Plastic Deformation in Aluminum Single Crystals," Trans. AIME, 221, 1206-1213 (1961).
6. S. K. Mitra and John E. Dorn, "On the Nature of Strain Hardening in Polycrystalline Aluminum and Aluminum-Magnesium Alloys," Trans. AIME, 227, 1015-1024 (1963)
7. W. Staubwasser, Thesis, University of Gottingen (1954); Acta Met., 7, 43 (1959).

8. A. C. Nunes, A. Rosen and J. E. Dorn, "Effect of Strain Hardening on the Low Temperature Thermally Activated Deformation Mechanisms in Polycrystalline Aluminum" accepted for publication in Trans. ASM.

9. J. Friedel, Dislocations (Pergamon Press, 1964) p. 61.

10. N. F. Mott, "Theory of Work Hardening in Metal Crystals" Phil. Mag. I, 43, 1151 (1952); "The Work Hardening of Metals," Trans. AIME, 218, 962 (1960).

11. Z. S. Basinski, "Thermally Activated Glide in F. C. C. Metals," Phil. Mag., 4, 393 (1959).

12. J. Friedel, "On the Linear Hardening Rate of F. C. C. Single Crystals," Phil. Mag., 46, 1196 (1955); Fracture (John Wiley, New York, 1959).

13. P. B. Hirsch, "Dislocation Distributions and Hardening Mechanisms in Metals, The Relation between the Structure and Mechanical Properties of Metals, (Her Majesty's Stationery Office, London, 1963) Vol. 1, p. 39.

14. D. Kuhlmann-Wilsdorf, "A New Theory of Work Hardening," Trans. AIME, 224, 1047 (1962).

15. W. M. Lomer, "A Dislocation Reaction in the F. C. C. Lattice," Phil. Mag., 42, 1327 (1951).

16. A. H. Cottrell, "Formation of Immobile Dislocations During Slip," Phil. Mag., 43, 645 (1952).

17. P. A. Jacquet, C. R. Acad. Sc., 239, 1799 (1954).

18. P. R. Swann, "Dislocation Arrangements in F. C. C. Metals and Alloys," Electron Microscopy and Strength of Crystals, ed. G. Thomas and J. Washburn (Interscience Publishers, New York, 1963) pp. 131-181.

19. P. B. Hirsch, "Observations of Dislocations in Metals," Internal Stresses and Fatigue in Metals, (Elsevier Publishing Co., Amsterdam, 1959) pp. 139-162.

20. D. Kuhlmann-Wilsdorf, R. Maddin and H. G. F. Wilsdorf, Strengthening Mechanisms in Solids, (ASM, Metals Park, Ohio, 1962) pp. 137-178.

APPENDIX A

Resolved Shear Strains and Shear Stresses on a Single Slip Plane During Polyslip

Let the axis of a tension bar be in the z direction and let x^i and z^i be the slip direction and the normal to the slip plane respectively for the ith slip system. During polyslip the incremental axial strain is

$$\frac{d\ell}{\ell} = d\varepsilon_{zz} = \sum_{i=1}^{n} \left(\alpha_{zx^i}\, \alpha_{zz^i}\, \frac{d\varepsilon_{x^i z^i}}{2} + \alpha_{zz^i}\, \alpha_{zx^i}\, \frac{d\varepsilon_{z^i x^i}}{2} \right)$$

$$= \sum_{i=1}^{n} \alpha_{zx^i}\, \alpha_{zz^i}\, d\varepsilon_{x^i z^i} \qquad \text{(A-1)}$$

where ℓ is the gage length of the specimens, the α's are the direction cosines between the directions indicated as subscripts and ε's are the strains denoted by the usual tensor subscript notation. The summation is taken over all operative systems from 1 to n. We consider here polyslip only for special orientations for which

$$\alpha_{zx^i}\, \alpha_{zz^i} = \alpha_{zx^j}\, \alpha_{zz^j} \qquad \text{(A-2)}$$

and

$$d\varepsilon_{x^i z^i} = d\varepsilon_{x^j z^j} = d\gamma$$

where γ is the shear strain on any one of the symmetrically disposed operative slip systems. Therefore

$$\frac{d\ell}{\ell} = n\alpha_{zx^i}\, \alpha_{zz^i}\, d\gamma = n \cos\lambda \sin\chi \qquad \text{(A-3)}$$

where λ and χ are the Schmid angles. When the above holds the orientations of crystals from C to F inclusive in Table I remains unchanged and A-3 can be integrated directly to give

$$\gamma = \frac{\ell n\, \ell/\ell_o}{n \sin\chi_o \cos\lambda_o} \quad \text{for C, D, E and F} \qquad \text{(A-4)}$$

Reorientation however takes place during slip for orientations A and B and, consequently, the direction cosines change during deformations.

As shown in Fig. A-1, a specimen of length ℓ_o increases in length to ℓ as it slips on the (111) plane in the $[\bar{1}01]$ direction. The transformation as point P_o moves to P is

$$(x - x_o) = -(z - z_o) \text{ and } y = y_o \tag{A-5}$$

Furthermore,

$$\cos\lambda = \left[\frac{x}{\ell}\ \frac{y_o}{\ell}\ \frac{z}{\ell}\right] \cdot \left[-\frac{1}{\sqrt{2}}\ 0\ \frac{1}{\sqrt{2}}\right] = \frac{-x+z}{\sqrt{2}\,\ell} \tag{A-6}$$

and

$$\sin\chi = \cos(90-\chi) = \left[\frac{x}{\ell}\ \frac{y_o}{\ell}\ \frac{z}{\ell}\right] \cdot \left[\frac{1}{\sqrt{3}}\ \frac{1}{\sqrt{3}}\ \frac{1}{\sqrt{3}}\right] = \frac{x + y_o + z}{\sqrt{3}\,\ell} \tag{A-7}$$

From A-5

$$x + y_o + z = x_o + y_o + z_o$$

and therefore A-7 becomes

$$\ell \sin\chi = \ell_o \sin\chi_o \tag{A-8}$$

Furthermore from A-5

$$x^2 + 2xz + z^2 = x_o^2 + 2x_oz_o + z_o^2 \tag{A-9}$$

and from A-6

$$x^2 - 2xz + z^2 = 2\,\ell^2 \cos^2\lambda \tag{A-10}$$

and

$$x_o^2 - 2x_oz_o + z_o^2 = 2\,\ell_o^2 \cos^2\lambda_o \tag{A-11}$$

whence

$$\ell \sin\lambda = \ell_o \sin\lambda_o \tag{A-12}$$

when A-8 and A-9 are introduced into A-3 for n = 1

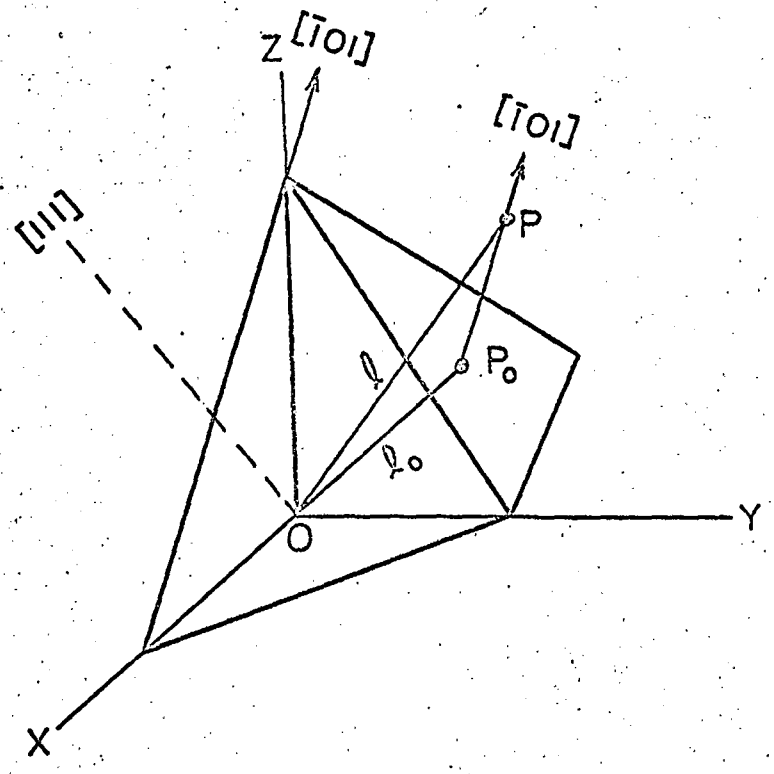

FIG. A-1 SINGLE SLIP.

$$d\gamma = \frac{d\ell}{\ell_o \sin\chi_o \sqrt{1 - \left|\frac{\ell_o}{\ell}\right|^2 \sin^2\lambda_o}} \qquad \text{(A-13)}$$

which upon integration yields

$$\gamma = \frac{\sqrt{\left|\ell/\ell_o\right|^2 - \sin^2\lambda_o} - \cos\lambda_o}{\sin\chi_o} \qquad \text{(A-14)}$$

The critical resolved shear stress for slip is always

$$\tau = L/A \sin\chi \cos\lambda \qquad \text{(A-15)}$$

where L and A are the instantaneous load and cross sectional area. For cases C to F of Table I, the angle χ and λ retain their original values and

$$\tau = \frac{L}{A_o}\frac{A_o}{A} \sin\chi_o \cos\lambda_o = \frac{L}{A_o}\left|\frac{\ell}{\ell_o}\right| \sin\chi_o \cos\lambda_o \qquad \text{(A-16)}$$

where the initial volume and final volumes $A_o\ell_o = A\ell$ are equal. For cases A and B of Table I, the area of the slip plane remains constant and

$$\tau = \frac{L\ell}{A_o\ell_o} \sin\chi \cos\lambda = \frac{L}{A_o} \sin\chi_o \sqrt{1 - \sin^2\lambda}$$

$$= \frac{L}{A_o} \sin\chi_o \sqrt{1 - \left|\frac{\ell_o}{\ell}\right|^2 \sin^2\lambda_o} \qquad \text{(A-17)}$$